CH Stretching Vibrational Overtone Spectra of *tert*-Butylbenzene, *tert*-Butyl Chloride, and *tert*-Butyl Iodide

Michael W. P. Petryk and Bryan R. Henry*

Department of Chemistry, University of Guelph, Guelph, Ontario N1G 2W1, Canada

Received: November 9, 2004

The vapor phase CH stretching vibrational overtone spectra of *tert*-butylbenzene and *tert*-butyl chloride are measured in the $\Delta v_{CH} = 2-7$ region, while the spectrum of *tert*-butyl iodide is recorded in the $\Delta v_{CH} = 2-6$ region. The overtone spectrum of *tert*-butylbenzene is too complex to make detailed spectral assignments. Local mode frequencies, $\tilde{\omega}$, and anharmonicities, $\tilde{\omega}x$, are obtained for *tert*-butyl chloride and *tert*-butyl iodide. The torsional dependencies of the local mode frequency, $\delta_{\tilde{\omega}}$, and anharmonicity, $\delta_{\tilde{\omega}x}$, are calculated for the *tert*-butyl halides. Nonbonded, through-space intramolecular interactions are observed in the blue-shifting of sterically hindered CH oscillators. Scaling factors are presented for relating ab initio calculated local mode parameters to experimental values for alkyl CH oscillators. Fermi resonances are observed between local mode states and local mode/normal mode combination states in *tert*-butyl chloride and *tert*-butyl iodide. Vibrational overtone transition intensities are calculated in the range $\Delta v_{CH} = 3-9$ using the harmonically coupled anharmonic oscillator (HCAO) model and ab initio dipole moment functions. The resultant HCAO intensities are compared to experimental intensities at $\Delta v_{CH} = 3$.

Introduction

The vibrational overtone stretching transitions of X−H bonds (X = C, N, O, etc.) are dominated by transitions to states whose components have all of their vibrational energy localized within one of a set of equivalent X−H oscillators. The localization of energy within local modes of vibration[1−5] makes overtone spectroscopy an extremely sensitive probe for detecting small changes in the properties of X−H bonds, such as bond lengths,[6−8] molecular conformations,[9,10] and energy flows in intramolecular vibrational energy redistribution (IVR).[11,12] In particular, it is possible to use overtone spectroscopy to probe how molecular geometry, and the amplitudes of local X−H vibrational modes, affect resonances, couplings, and the rate of IVR.

The molecular Hamiltonian can be expressed in a local mode basis, which leads to X−H stretch terms for which off-diagonal coupling elements are small compared to the (anharmonic) diagonal cubic and quartic terms.[13] The contributions of the diagonal terms become increasingly dominant with increasing vibrational excitation. It is therefore possible to treat the potential of a molecule as a collection of isolated anharmonic oscillators in which coupling between oscillators is treated as a perturbation.[11] Often the anharmonic oscillators are approximated using Morse oscillator expressions because the energies and matrix elements of the Morse oscillator wave function have been solved analytically.[4,14]

The basis states for *n*XH Morse oscillators can be written as a product of individual one-dimensional Morse wave functions $|v_1\rangle|v_2\rangle...|v_i\rangle...|v_n\rangle$ or simply as $|v_1,v_2,...,v_i,...,v_n\rangle$, where v_i is the number of vibrational quanta in the *i*th X−H oscillator. Spectrally "bright" states, i.e., those states which carry intensity from the $v = 0$ vibrational state, are almost exclusively pure local mode states which can be described by a linear combination of components in which all of the vibrational energy is localized in one oscillator (e.g., $|v, 0,..., 0\rangle$, $|0,v,..., 0\rangle$, etc.). In the case where the local methyl group has C_s symmetry, the pure local mode wave function of the unique X−H oscillator is denoted $|0, 0\rangle|v\rangle$. The pure local mode wave functions of the two identical coupled X−H oscillators are the symmetric $|v, 0\rangle_+|0\rangle$ state and the antisymmetric $|v, 0\rangle_-|0\rangle$ state. Symmetrized wave functions become increasingly degenerate with increasing excitation so that symmetry effects are generally not observed where three or more vibrational quanta have been absorbed by the X−H oscillator, i.e., where $\Delta v_{XH} \geq 3$. The nearly degenerate symmetric and antisymmetric states that cannot be resolved from one another can be collectively denoted as $|v, 0\rangle_\pm|0\rangle$. The local mode description has been extended to multioscillator systems in the harmonically coupled anharmonic oscillator (HCAO) model.[5,15−17]

Previous studies have reported that the CH stretching potentials become more harmonic with increases in steric crowding.[18−20] Steric crowding has been reported to give rise to intramolecular coupling through space between proximal, nonbonded atoms in neopentane, $C(CH_3)_4$.[21] This coupling through space can enhance Fermi resonances, thereby accelerating IVR and leading to complex spectral features.

Another mechanism by which CH oscillators are perturbed is via halogen substitution. Studies on dihalomethanes indicate that the CH force constant increases with halogen substitution[22] and that the local mode frequency, $\tilde{\omega}$, increases with increasing electronegativity.[23]

The purpose of this paper is to investigate the roles of steric crowding and halogen substitution on the local mode properties of CH oscillators and on through-space coupling. Specifically, we are interested in whether through-space interactions, in which the van der Waals spheres of proximal, nonbonded atoms interact to render the CH stretching potential more harmonic, are a general phenomenon or if they are restricted to $M(CH_3)_4$ homologues.[21] We will investigate the vibrational overtone spectra of *tert*-butylbenzene, *tert*-butyl chloride, and *tert*-butyl iodide. The overtone transitions of *tert*-butyl chloride were

10.1021/jp040710h CCC: $30.25
Published on Web 04/15/2005

studied previously[24] in the liquid ($\Delta v_{CH} = 1-6$) and vapor phases ($\Delta v_{CH} = 1-4$). In this paper we extend the experimental range through $\Delta v_{CH} = 7$ in the vapor phase.

Experimental Section

Sample Preparation. All of the compounds are liquids. *tert*-Butylbenzene (Aldrich, 99%), *tert*-butyl chloride (Aldrich, 99%), and *tert*-butyl iodide (Aldrich, 95%, stabilized with copper) were degassed by repeated freeze−pump−thaw cycles prior to use.

Owing to the low vapor pressures of *tert*-butylbenzene, argon gas (Cannox, 99%) was used to (1) carry the sample through the vacuum line into the evacuated photoacoustic (PA) cell, and (2) act as a "buffer" gas in aiding the propagation of the acoustic signal. The argon was slowly passed through Drierite (which had been dried by heating under vacuum) and introduced into the vacuum vial containing the sample. The sample/argon mixture was allowed to equilibrate for at least 2 h before the gas mixture was allowed to expand into an evacuated PA cell (vide infra). The final pressure of the argon gas ranged from 100 Torr to 700 Torr.

Intracavity Laser Photoacoustic Spectroscopy. Our ICL-PAS setup has been described elsewhere.[25,26] In summary a 20 W Coherent Innova 200 argon ion laser is used to pump a Coherent 599 tunable dye laser or a broadband Coherent 890 Ti:sapphire (Ti:sapph) laser. In this work we use the short wave and mid wave optics in the Ti:sapph laser, and the laser dyes DCM and Coumarin 6. This combination enabled us to scan a region from 9300 to 19 000 cm^{-1} ($\Delta v_{CH} = 4-7$). Tuning is accomplished using birefringent filters which have resolutions of approximately 0.4 cm^{-1}. Spectra are referenced to known water lines,[27] resulting in an estimated error in peak position of less than 2 cm^{-1}. The gas line and PA cell are evacuated to a pressure of 10^{-4} to 10^{-5} Torr for at least 4 h prior to sample introduction to ensure dryness.

Theory and Calculations

Local Modes of Vibration and the HCAO Model. X−H stretching overtone spectra can be interpreted within the local mode model of molecular vibration.[2,3] Within this model the X−H stretching potential is often approximated by a Morse potential[11]

$$V(q) = D_e(1 - e^{-aq})^2 \tag{1}$$

where q is the displacement from the equilibrium X−H bond length, D_e is the depth of the potential well, and a is the Morse scaling factor. The energy eigenvalues of a Morse oscillator, $\tilde{E}_v$, are[11,28]

$$\tilde{E}_v = \tilde{\omega}\left(v + \frac{1}{2}\right) - \tilde{\omega}x\left(v + \frac{1}{2}\right)^2 \tag{2}$$

where $\tilde{\omega}$ is the local mode frequency and $\tilde{\omega}x$ is the local mode anharmonicity. Equation 2 can be rearranged to give the frequency, $\tilde{\nu}_{v\leftarrow 0}$, of an overtone transition (from the ground state) $(v' = v) \leftarrow (v'' = 0)$[11]

$$\tilde{\nu}_{v\leftarrow 0} = v\omega - (v^2 + v)\tilde{\omega}x \tag{3}$$

The values of the Morse parameters $\tilde{\omega}$ and $\tilde{\omega}x$ are obtained from a quadratic fit of $\tilde{\nu}_{v\leftarrow 0}$ vs v or from a Birge−Sponer plot of $\tilde{\nu}_{v\leftarrow 0}/v$ vs v. The eigenstates are obtained within the HCAO model[5,15−17] in terms of Morse oscillator wave functions[11] with the assumption of harmonic coupling between the X−H oscillators.

Force Constants and Their Relationship to Morse Oscillator Parameters. Sowa et al.[29] showed that an isolated X−H oscillator could be expressed as

$$V(q) = \frac{1}{2}f_{ii}q^2 + \frac{1}{6}f_{iii}q^3 + \frac{1}{24}f_{iiii}q^4 \tag{4}$$

where f_{ii}, f_{iii}, and f_{iiii} are the quadratic, cubic, and quartic diagonal X−H force constants, respectively. Correspondences between the Morse parameters and the diagonal force constants are[29]

$$\tilde{\omega} = \frac{\sqrt{G_{ii}f_{ii}}}{2\pi c} \tag{5}$$

and

$$\tilde{\omega}x = \frac{hG_{ii}}{72\pi^2 c}\left(\frac{f_{iii}}{f_{ii}}\right)^2 \tag{6}$$

where G_{ii} is the Wilson **G**-matrix element (vide infra).

Three Coupled Methyl Oscillators. The (unsymmetrized) wave function of three coupled local mode CH oscillators excited by v vibrational quanta can be expressed as $|v, 0, 0\rangle$. The frequencies of transitions out of the ground $|0, 0, 0\rangle$ state to the states $|v, 0, 0\rangle$ are[5]

$$\frac{H - E_{|0,0,0\rangle}}{hc} = \sum_i^3 v_i\tilde{\omega}_i - \sum_i^3 (v_i^2 + v_i)\tilde{\omega}x_i - \sum_{i\neq j}^3 \gamma'_{ij}(a_i a_j^+ + a_i^+ a_j) \tag{7}$$

where $E_{|0,0,0\rangle}$ is the energy of the vibrational ground state and γ'_{ij} is the intramanifold coupling parameter[5]

$$\gamma'_{ij} = (\gamma_{ij} - \phi_{ij})\sqrt{\tilde{\omega}_i\tilde{\omega}_j} \tag{8}$$

where γ_{ij} and ϕ_{ij} are, respectively, the kinetic and potential energy coupling terms. These terms can be expressed as[5]

$$\phi_{ij} = \frac{1}{2}\frac{F_{ij}}{F_{ii}F_{jj}} \tag{9}$$

and

$$\gamma_{ij} = -\frac{1}{2}\frac{G_{ij}}{G_{ii}G_{jj}} \tag{10}$$

γ_{ij} is a function of molecular conformation only, and can be expressed as[5]

$$\gamma_{ij} = -\frac{1}{2}\cos(\theta)\left(1 + \frac{m_C}{m_H}\right)^{-1} \tag{11}$$

where θ is the H−C−H bond angle and m_C and m_H are the atomic masses of C and H.

Spectral Manifestations of Fermi Resonances. Energy can flow out of an initially prepared pure local mode state, $|v, 0, 0\rangle$, into a near-resonant local mode-normal mode combination state $|v - 1, 0, 0\rangle|nv_b\rangle$ (where $|nv_b\rangle$ denotes n vibrational quanta, typically deposited in a bending mode $|v_b\rangle$). Energy flow

between a pure local mode state and a near-resonant combination state can be observed as a splitting in the frequency domain caused by a mixing between the wave functions[12] where the magnitude of the splitting reflects the rate of vibrational energy flow.[30] This spectral splitting arises from Fermi resonance.[31] The frequency of the (isolated) state $|v, 0, 0\rangle$ in the absence of this perturbing interaction, $\tilde{\nu}_{\mathrm{iso}}$, is approximated by the average of the perturbed energies of the observed local mode and combination peaks, $\tilde{\nu}_{\mathrm{lm}}$ and $\tilde{\nu}_{\mathrm{comb}}$, weighted by their relative intensities[32]

$$\tilde{\nu}_{\mathrm{iso}} = \frac{\tilde{\nu}_{\mathrm{lm}} f_{\mathrm{lm}} + \tilde{\nu}_{\mathrm{comb}} f_{\mathrm{comb}}}{f_{\mathrm{lm}} + f_{\mathrm{comb}}} \tag{12}$$

where f_{lm} and f_{comb} denote the intensities of the observed local mode and combination peaks, respectively.

Oscillator Strength. The experimental intensities of vibrational overtone transitions are conveniently expressed in terms of the dimensionless oscillator strength, f.[33] By applying the ideal gas law and using the appropriate physical constants,[34] we obtain an expression for f in the form

$$f = 2.6935 \times 10^{-9}(\mathrm{Torr\ m\ cm}) \frac{T}{p\,l} \int A(\tilde{\nu}_{\mathrm{eg}})\, \mathrm{d}(\tilde{\nu}_{\mathrm{eg}}) \tag{13}$$

where T is the temperature of the gas expressed in Kelvin, p is the gas pressure expressed in Torr, l is the path length expressed in meters, and $A(\tilde{\nu}_{\mathrm{eg}})$ is the absorbance of the transition from ground state g to excited state e as a function of frequency, $\tilde{\nu}_{\mathrm{eg}}$, in wavenumbers ($\mathrm{cm}^{-1}$). The integration is carried out over the frequency range of the absorption feature.

The oscillator strength of an overtone transition can be calculated in terms of the transition frequency, $\tilde{\nu}_{\mathrm{eg}}$, the transition dipole moment function, μ_{eg}, and some physical constants.[33] The transition dipole moment matrix element in Debye is given by

$$\mu_{\mathbf{eg}} = \langle e|\vec{\mu}|g\rangle \tag{14}$$

where e and g are the excited and ground-state wave functions respectively, and $\vec{\mu}$ is the DMF. The Morse wave function for an X−H oscillator excited by v vibrational quanta can be determined from the reduced mass μ and the local mode parameters $\tilde{\omega}$ and $\tilde{\omega}x$.[11] Using the appropriate physical constants,[34] the oscillator strength of an overtone transition can be expressed as[33]

$$f = 4.70175 \times 10^{-7}(\mathrm{cm\ D}^{-2})\tilde{\nu}_{\mathrm{eg}}|\mu_{\mathrm{eg}}|^2 \tag{15}$$

The Dipole Moment Function. The coupling between the methyl CH oscillators (vide supra) is treated within the HCAO model as pairwise interactions between the internal displacement coordinates q_1 along CH_1 and q_2 along CH_2. Ab initio calculations have been used[35−39] to obtain discrete values for the dipole moment as a function of q_1 and q_2. In this paper, the values of the dipole moment were calculated as q_1 and q_2 were stretched or compressed about the equilibrium X−H bond length r_e by ±0.20 Å in increments of 0.05 Å with all other molecular coordinates constant at their equilibrium values. The continuous DMF of two coupled X−H oscillators is approximated by a Taylor series expansion, taken up to fourth order, along their internal stretch coordinates q_1 and q_2

$$\vec{\mu}(q_1, q_2) = \sum_{i,j=1}^{i+j=4} \vec{\mu}_{ij} {q_1}^i\, {q_2}^j \tag{16}$$

where $\vec{\mu}_{ij}$ are the DMF derivatives

$$\vec{\mu}_{ij} = \frac{1}{i!j!} \frac{\partial^{i+j}\vec{\mu}}{\partial {q_1}^i \partial {q_2}^j}\bigg|_{\mathrm{e}} \tag{17}$$

which were obtained by fitting a polynomial of up to fourth order to ab initio values of the dipole moment. Terms up to fourth order were retained in eq 16, including the pairwise mixed derivatives $\partial^2\vec{\mu}/\partial {q_1}^1 \partial {q_2}^1$, $\partial^3\vec{\mu}/\partial {q_1}^1 \partial {q_2}^2$, and $\partial^3\vec{\mu}/\partial {q_1}^2 \partial {q_2}^1$. It is especially important to include terms beyond linear as the second-order derivatives $\partial^2\vec{\mu}/\partial {q_1}^2$ and $\partial^2\vec{\mu}/\partial {q_2}^2$ contribute significantly more intensity to overtone transitions than do the linear terms.

Computational Details. Ab initio calculations were carried out with Gaussian 98 revision A.5[40] on an SGI Octane with a MIPS R10000 processor, Gaussian 98 revision A.11[41] on a cluster with Compaq Alpha ES40 (4 × 833 MHz) processors, and Gaussian 03W revision B.03[42] on a personal computer with a Pentium 4, 2.8 GHz processor. Calculations used all Gaussian defaults (unless noted otherwise) except that the Gaussian overlay option IOP(3/32 = 2) was used with all calculations to prevent the reduction of expansion sets. All calculations were carried out using SCF = tight because many of the basis sets used in this paper contained diffuse functions.

Results and Discussion

General Characteristics of Vibrational Overtone Spectra and Spectral Fitting. In the absence of coupling, one stretching overtone transition peak is observed for each nonequivalent X−H bond where the frequency of that transition is given by eq 3. Experimental spectra are deconvoluted in SpectraCalc[43] with the least number of constituent peaks needed to reproduce the experimental spectrum. The sum of the constituent peaks reproduces closely the experimental transitions: the maximum standard deviations introduced in the peak centers, heights, and full-widths at half-maximum (fwhm) by the peak fitting process were found to be, respectively, 3 cm^{-1}, 3%, and 6%. All spectral deconvolutions use Lorentzian profiles as constituent peaks. For PA spectra, the constituent Lorentzian peak heights and widths are independently scaled to sum to unity in a given spectral range. Their absolute values range over several orders of magnitude, are dependent upon several factors, and offer no important information. In cases where more than one Lorentzian is required to deconvolute a vibrational overtone transition, the dominant Lorentzian is chosen to represent the pure local mode transition. If there are two or more Lorentzians of comparable intensity the Lorentzian chosen to represent the pure local mode transition is the one that gives the most linear Birge−Sponer plot. The "isolated" transition frequencies of pure local mode transitions which are perturbed by Fermi resonances are approximated with eq 12.

Owing to the very short lifetimes of the prepared vibrational overtone states, collisional deactivation is not appreciable at our experimental temperatures and pressures.[21] Dephasing is likewise unimportant as the local environment does not fluctuate rapidly compared to the lifetime of the excited state.

***tert*-Butylbenzene.** The global minimum potential energy conformation of *tert*-butylbenzene possesses C_s symmetry, with one carbon to methyl carbon bond in the plane of the benzene ring. The in-plane methyl group possesses local C_s symmetry while the two out-of-plane methyl groups possesses local C_1 symmetry. There are are 10 different CH oscillators in *tert*-butylbenzene, many of which are expected to have very similar vibrational overtone frequencies. The inherent breadth of CH

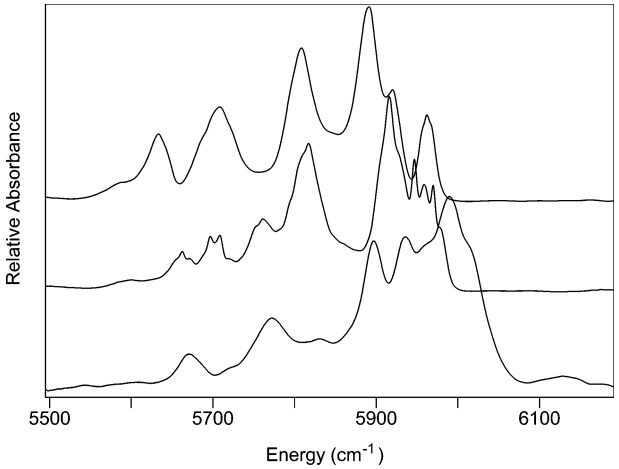

Figure 1. $\Delta v_{CH} = 2$ region of the Cary/5e vapor phase spectrum of *tert*-butyl iodide (top), *tert*-butyl chloride (middle), and *tert*-butylbenzene obtained at a path length of 20.25 m. Sample pressures were, respectively, 15.4, 20.8, and 1.7 Torr while temperatures ranged from 22.2 to 22.7 °C.

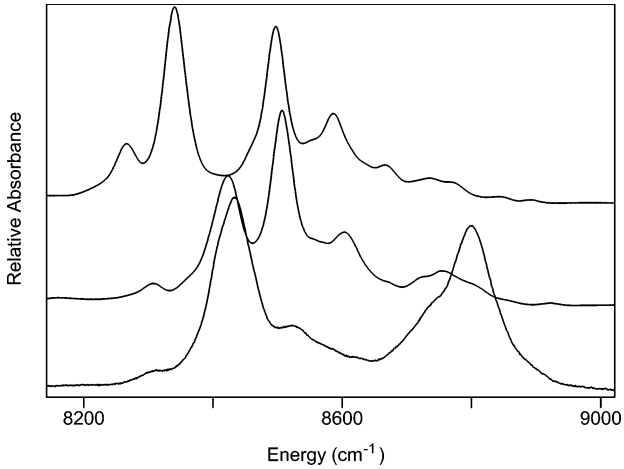

Figure 2. $\Delta v_{CH} = 3$ region of the Cary/5e vapor phase spectrum of *tert*-butyl iodide (top), *tert*-butyl chloride (middle), and *tert*-butylbenzene obtained at a path length of 20.25 m. Sample pressures were, respectively, 15.4, 102.7, and 1.7 Torr while temperatures ranged from 22.0 to 22.4 °C.

overtone transitions is such that, even in the absence of Fermi resonance, the unique assignment of all CH overtone transitions based solely upon the $\Delta v_{CH} = 2-7$ spectral regions is impossible, irrespective of experimental resolution.

The geometry of the C_s symmetry conformer of *tert*-butylbenzene is calculated using HF and B3LYP theory with the basis sets 6-31G(d,p) and 6-311++G(2d,2p). Calculations are also carried out using B3LYP theory with the cc-pVDZ and cc-pVTZ basis sets. The hydrogen−hydrogen internuclear separation through space, δ_{HH}, between the proximal hydrogen atoms on two different methyl groups was found to range from 2.45 to 2.47 Å. The crowding is greater between proximal atoms where one hydrogen is on the methyl group and the other on the aryl ring. For the in-plane methyl group, δ_{HH} was calculated to range from 2.27 to 2.28 Å while for the out-of-plane methyl group, δ_{HH} was calculated to range from 2.30 to 2.31 Å. The van der Waals radius for hydrogen is 120 pm.[44] Methyl-aryl δ_{HH} values are smaller than the sum of two van der Waals hydrogen radii, and thus strong steric crowding is expected to exist in *tert*-butylbenzene.

The $\Delta v_{CH} = 2$ and $\Delta v_{CH} = 3$ alkyl spectral regions of *tert*-butylbenzene, shown in Figures 1 and 2 respectively, are rich with many complex resonances. The $\Delta v_{CH} = 4$ alkyl spectral region is shown in Figure 3. This figure reveals the five aryl C−H oscillators to be unresolved within two strong transitions at ca. 11190 and 11250 cm^{-1} while the remaining five alkyl C−H oscillators are unresolved within approximately three weak, broad transitions at ca. 10950, 11010, and 11070 cm^{-1}. The alkyl transitions are broader than the aryl transitions because IVR is more rapid in the former than in the latter owing to methyl rotor coupling (via Fermi resonance) into local mode-normal mode combination states. This coupling is enhanced by steric hindrance.[21] At all overtones, the lowest frequency aryl transitions occur at lower frequencies than are typical of aryl C−H oscillators (see ref 45). In Figure 4 we note the alkyl regions (ca. 13400 to 13700 cm^{-1}) are again broader than the aryl regions (i.e., above 13700 cm^{-1}), with the difference in the fwhm values even more pronounced than at $\Delta v_{CH} = 4$. While the lifetimes of the aryl C−H overtones appear unchanged in moving from $\Delta v_{CH} = 4$ to $\Delta v_{CH} = 5$, the alkyl lifetimes appear to be shortened. The large amplitude stretching motions which accompany vibrational overtone transitions appear to have a strong effect on alkyl CH stretching overtone lifetimes. The

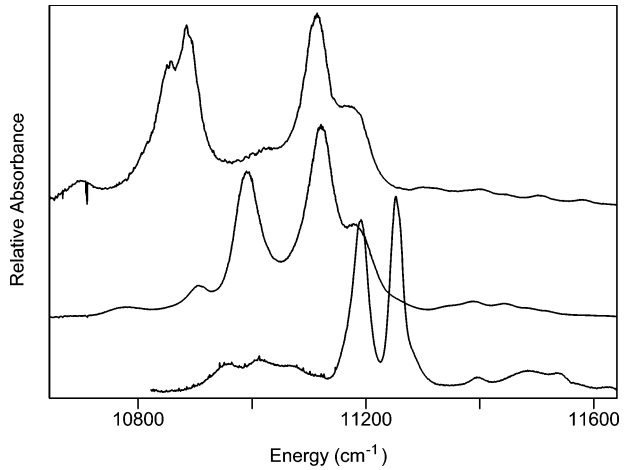

Figure 3. ICL-PAS (Ti:sapph (mw)) $\Delta v_{CH} = 4$ region of the vapor phase spectrum of *tert*-butyl iodide (top), *tert*-butyl chloride (middle), and *tert*-butylbenzene. *tert*-Butyl iodide and *tert*-butyl chloride were present at pressures of 34.7 ± 0.8 Torr and 93.8 ± 1.4 Torr, respectively, at 21.0 °C. *tert*-Butylbenzene was present at its vapor pressure at 21.0 °C.

aryl $\Delta v_{CH} = 6$ and $\Delta v_{CH} = 7$ spectral regions are shown in Figures 5 and 6, respectively. The $\Delta v_{CH} = 7$ aryl region has a very poor signal-to-noise ratio owing to very low sample vapor pressure and to the residual presence of water vapor, despite thorough drying of the sample. Features below 18500 cm^{-1} and above 19020 cm^{-1} are completely obscured by water vapor.

***tert*-Butyl Chloride.** In its equilibrium geometry *tert*-butyl chloride possesses C_{3v} symmetry with local C_s symmetry for the methyl groups. There are two types of nonequivalent CH oscillators in *tert*-butyl chloride. Three identical CH bonds are oriented opposite the C−Cl bond and are referred to as the "down" oscillators, CH_d. Six identical CH bonds are oriented at a dihedral angle of approximately 60° to the C−Cl bond and are referred to as the "up" oscillators, CH_u.[24]

The geometry of the equilibrium conformer of *tert*-butyl chloride is calculated using HF and B3LYP theory with the basis sets 6-31G(d,p), 6-311++G(2d,2p), LanL2MB, LanL2DZ, cc-pVDZ, cc-pVTZ, and cc-pVQZ. The chlorine−hydrogen internuclear separation through space, δ_{ClH}, between the proximal (or "up") hydrogen atoms and the chlorine atom was found to range from 2.89 to 2.92 Å for both the Pople and Dunning basis

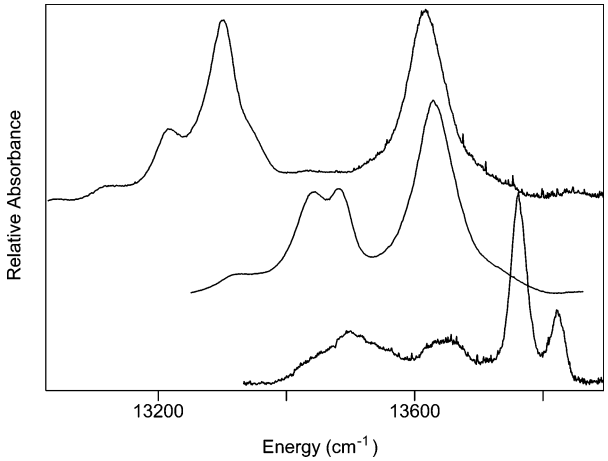

Figure 4. ICL-PAS (Ti:sapph (sw)) $\Delta v_{CH} = 5$ region of the vapor phase spectrum of *tert*-butyl iodide (top), *tert*-butyl chloride (middle), and *tert*-butylbenzene. *tert*-Butyl iodide and *tert*-butyl chloride were present at pressures of 34.6 ± 0.7 and 128.2 ± 0.9 Torr, respectively, and temperatures of 21.9 and 22.0 °C. *tert*-Butylbenzene was present at its vapor pressure at 23.8 °C in a cell that contained approximately 200 Torr of dried Ar buffer gas.

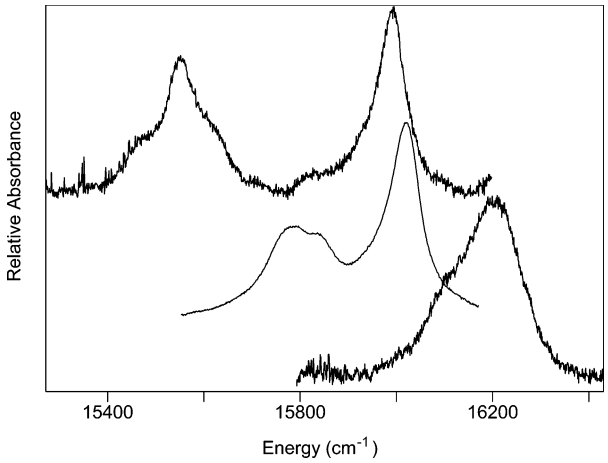

Figure 5. ICL-PAS (DCM dye) $\Delta v_{CH} = 6$ region of the vapor phase spectrum of *tert*-butyl iodide (top), *tert*-butyl chloride (middle), and *tert*-butylbenzene. *tert*-Butyl iodide and *tert*-butyl chloride were present at pressures of 144.8 ± 0.2 and 31.7 ± 0.3 Torr, respectively, and temperatures of 22.0 and 22.1 °C. *tert*-Butylbenzene was present at its vapor pressure at 22.1 °C in a cell that contained approximately 200 Torr of dried Ar buffer gas.

sets and from 2.94 to 2.99 Å for the Los Alamos basis sets. The δ_{ClH} values are smaller than the sum of hydrogen and chlorine van der Waals radii, which are 120 pm and 180 pm,[44] respectively. Through-space interactions are expected perturb the stretching potential of CH_u more strongly than that of CH_d.

Simple, two-tier Fermi resonances are present throughout the entire experimental range of $\Delta v_{CH} = 2-7$. In such resonances, the pure local mode state $|v, 0, 0\rangle$ tunes in to and out of resonance[46,47] with the normal mode-local mode combination state $|v - 1, 0, 0\rangle + |nv_b\rangle$ as we proceed through the progression of overtone states from $\Delta v_{CH} = 2$ to $\Delta v_{CH} = 7$. This trend arises from the anharmonicity of the CH local mode oscillator which results in a smaller spacing between successive pure local mode states than between successive resonant combination states. As the energy mismatch between the states becomes smaller, the separation between the pure local mode and the combination transitions decreases.[46,47]

The $\Delta v_{CH} = 2$ spectral region, shown in Figure 1, has many local mode-normal mode combination bands and is too complex

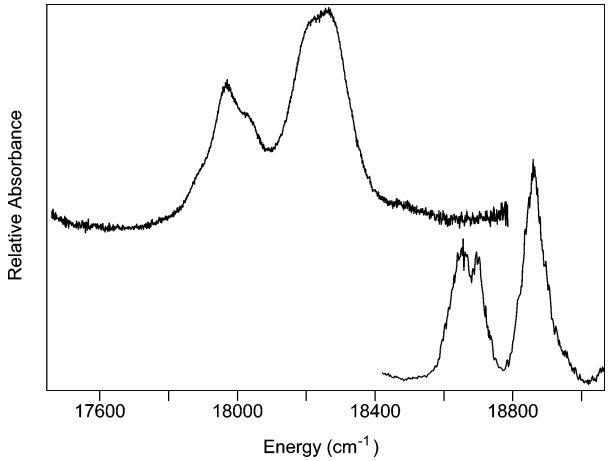

Figure 6. ICL-PAS (C6 dye) $\Delta v_{CH} = 7$ region of the vapor phase spectrum of *tert*-butyl chloride (top) and *tert*-butylbenzene. *tert*-Butyl chloride was present at its vapor pressure at a temperature of 24.8 °C. *tert*-Butylbenzene was present at its vapor pressure at a temperature of 22.0 °C in a cell that contained approximately 200 Torr of dried Ar buffer gas.

for local mode analysis. In Figure 2 we observe that there is one $\Delta v_{CH} = 3$ transition to the pure local mode state $|0, 0\rangle|3\rangle$ (in the CH_d oscillator) at 8420 cm^{-1}. There is a local mode/local mode-normal mode combination pair involving the $|3, 0\rangle_{\pm}|0\rangle$ and $|2, 0\rangle_{\pm}|0\rangle + |nv_b\rangle$ states of the CH_u oscillator at 8507 and 8606 cm^{-1}, respectively. These three transitions comprise the most intense transitions observed at $\Delta v_{CH} = 3$ in Figure 2. Similarly, in Figure 3 we note that there is one $\Delta v_{CH} = 4$ pure local mode transition to $|0, 0\rangle|4\rangle$ in the CH_d oscillator at 10992 cm^{-1} and a local mode/local mode-normal mode combination pair to $|3, 0\rangle_{\pm}|0\rangle + |nv_b\rangle$ and $|4, 0\rangle_{\pm}|0\rangle$ in the CH_u oscillator at 11190 and 11120 cm^{-1}, respectively. These three transitions comprise the most intense transitions observed at $\Delta v_{CH} = 4$. Other resonances at $\Delta v_{CH} = 4$ are less pronounced than those at $\Delta v_{CH} = 3$ as the CH oscillations take on increasing local mode character. The two resonant CH_u transitions which were present at $\Delta v_{CH} = 4$ are seen in Figure 4 to have coalesced at $\Delta v_{CH} = 5$ into one peak at 13631 cm^{-1}. A $|0, 0\rangle|4\rangle + |nv_b\rangle$ combination band transition arising from the CH_d oscillator appears at 13485 cm^{-1}, near the transition to the $|0, 0\rangle|5\rangle$ state at 13439 cm^{-1}. The $\Delta v_{CH} = 6$ spectral region, shown in Figure 5, has transitions to the $|0, 0\rangle|6\rangle$ and $|0, 0\rangle|5\rangle + |nv_b\rangle$ states at 15776 and 15845 cm^{-1}, respectively. The $|v_b\rangle$ state involved at $\Delta v_{CH} = 6$ is different than that at $\Delta v_{CH} = 5$. Had the state $|v_b\rangle$ remained unchanged, we would expect to have seen the spacing between the $|0, 0\rangle|v\rangle$ and $|0, 0\rangle|v - 1\rangle + |nv_b\rangle$ states decrease in going from $\Delta v_{CH} = 5$ to $\Delta v_{CH} = 6$. Instead, the spacing increases from 46 cm^{-1} at $\Delta v_{CH} = 5$ to 69 cm^{-1} $\Delta v_{CH} = 6$. The CH_u transitions which had coalesced at $\Delta v_{CH} = 5$ have separated into two poorly resolved $\Delta v_{CH} = 6$ transitions, $|6, 0\rangle_{\pm}|0\rangle$ and $|5, 0\rangle_{\pm}|0\rangle + |nv_b\rangle$, at 15976 and 16022 cm^{-1}, respectively, where the lower energy peak appears as a shoulder in the deconvolution of the spectrum.[48] A resonance between the $|6, 0\rangle_{\pm}|0\rangle + |nv_b\rangle$ transition at 18281 cm^{-1} and the $|7, 0\rangle_{\pm}|0\rangle$ transition at 18203 cm^{-1} can be seen in the $\Delta v_{CH} = 7$ region, Figure 6. Transitions to the $|0, 0\rangle|7\rangle$ and $|0, 0\rangle|6\rangle + |nv_b\rangle$ states can be seen at 17965 and 18035 cm^{-1}, respectively. The $\Delta v_{CH} = 7$ transitions of the CH_u and CH_d oscillators both involve $|v_b\rangle$ states different from those involved in the $\Delta v_{CH} = 6$ transitions. In the case of the CH_u oscillator, this is evident because the local mode-normal mode combination band appears at the high energy side of the local mode band. In the case of the CH_d oscillator, the spacing between the local mode and the

TABLE 1: Pure Local Mode Transition Peak Properties of Vapor Phase *tert*-Butyl Chloride As Observed via ICL-PAS ($\Delta v_{CH} = 4-7$) and Conventional Absorption Spectroscopy ($\Delta v_{CH} = 3$)

Δv_{CH}	spectrometer/ laser	gas pressure (Torr)	bond	energy[a] (cm^{-1})	fwhm[a,b] (cm^{-1})
3	Cary 5e	102.7 ± 0.2	CH_u	8507, *8606*	41, *64*
			CH_d	8420	53
4	Ti:sapph (mw)	93.8 ± 1.4	CH_u	11120, *11191*	62, *54*
			CH_d	10 992	53
5	Ti:sapph (sw)	128.2 ± 0.9	CH_u	13 631	77
			CH_d	13439, *13485*	66, *38*
6	DCM dye	144.8 ± 0.2	CH_u	*15976*, 16022	*128*, 66
			CH_d	15776, *15845*	114, *77*
7	coumarin 6 dye	$\simeq 160$ [c]	CH_u	*18203*, 18281	*128*, 110
			CH_d	17965, *18035*	93, *83*

[a] Italicized values are for $|v - 1, 0, 0\rangle + |nv_b\rangle$. [b] Full width at half-maximum. [c] Sample present at its vapor pressure at 24.8 °C

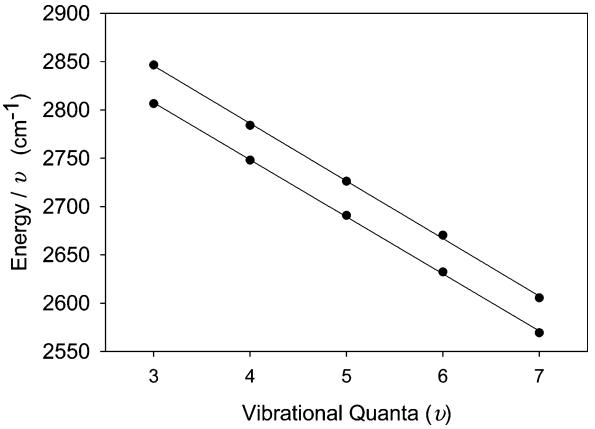

Figure 7. Birge−Sponer plots of the CH_u (top) and CH_d vibrational overtone transitions in *tert*-butyl chloride in the range $\Delta v_{CH} = 3-7$.

TABLE 2: Experimental[a] Local Mode Parameters and Their Standard Deviations (in cm^{-1}) As Obtained from Birge−Sponer Plots and Quadratic Fits

		Birge−Sponer		quadratic	
molecule	bond	$\tilde{\omega}$	$\tilde{\omega}x$	$\tilde{\omega}$	$\tilde{\omega}x$
tert-butyl chloride	CH_u	3084 ± 4	59.6 ± 0.8	3085 ± 7	59.8 ± 1.2
	CH_d	3044 ± 3	59.0 ± 0.6	3047 ± 5	59.5 ± 0.9
tert-butyl iodide	CH_u	3081 ± 2	59.5 ± 0.3	3080 ± 3	59.3 ± 0.5
	CH_d	3025 ± 5	61.3 ± 1.1	3026 ± 9	61.5 ± 1.8
neopentane-d_0[b]		3046 ± 2	60.1 ± 0.3	3049 ± 3	60.5 ± 0.4
TMS[b]		3043 ± 1	58.6 ± 0.2	3042 ± 2	58.4 ± 0.3

[a] Calculated from experimental data in the energy regime $\Delta v_{CH} = 3-7$ except for *tert*-butyl iodide where the energy regime is $\Delta v_{CH} = 3-6$. [b] From ref 55.

local mode−normal mode combination band is nearly invariant from 69 cm^{-1} at $\Delta v_{CH} = 6$ to 70 cm^{-1} at $\Delta v_{CH} = 7$ rather than growing smaller as the states come into resonance with increasing vibrational excitation.

A summary of the $\Delta v_{CH} = 3-7$ transitions of *tert*-butyl chloride can be seen in Table 1. Italicized values indicate the combination state $|v - 1, 0, 0\rangle + |nv_b\rangle$. The data in Table 1 have been used to create Birge−Sponer plots, which are presented in Figure 7, for the CH_u and CH_d oscillators in *tert*-butyl chloride with peak centers (in the absence of Fermi resonance) approximated with eq 12. Table 2 gives the local mode parameters $\tilde{\omega}$ and $\tilde{\omega}x$ which were obtained via quadratic fits and Birge−Sponer regressions. The $\tilde{\omega}$ values are higher for the more sterically crowded CH_u oscillator than for the less crowded CH_d oscillator. The anharmonicities of the "up" and "down" CH oscillators are identical to within experimental error. In Table 2, we note that the $\tilde{\omega}$ value of the CH_d oscillator is typical of that observed in molecules such as neopentane and tetramethylsilane (TMS). The $\tilde{\omega}$ value of the CH_u oscillator is atypically high, and it is attributed to a combination of steric crowding and a possible increase in the CH force constant by the halogen.[22,23]

***tert*-Butyl Iodide.** The structure of *tert*-butyl iodide is similar to that of its homolog, *tert*-butyl chloride (vide supra). *tert*-Butyl iodide possesses C_{3v} symmetry with local methyl C_s symmetry. As in the case of *tert*-butyl chloride, a molecule of *tert*-butyl iodide possesses three CH_d oscillators and six CH_u oscillators.

The geometry of the equilibrium conformer of *tert*-butyl iodide is calculated using HF and B3LYP theory with the LanL2MB and LanL2DZ basis sets (the 6−311 basis set is not defined for iodine). The iodine−hydrogen internuclear separation through space, δ_{IH}, between the proximal (or "up") hydrogen atoms and the iodine atom was found to range from 3.21 to 3.27 Å. The δ_{IH} values are smaller than the sum of hydrogen and iodine van der Waals radii, which are 120 pm and 215 pm,[44] respectively. Through-space interactions are expected to perturb the stretching potential of CH_u more strongly than that of CH_d.

The vapor phase CH vibrational overtone transitions of *tert*-butyl iodide were studied in the range $\Delta v_{CH} = 2-6$. The sample began to photodissociate at $\Delta v_{CH} = 6$. Vibrational overtone spectra at $\Delta v_{CH} = 7$ or greater are impossible to obtain with our experimental setup as the molecule decomposes within seconds in this frequency range.

Photodissociation was first noticed at $\Delta v_{CH} = 6$ in the approximate energy range 14040−16460 cm^{-1} at a temperature of 22 °C. The dissociation energy of the C−I bond in *tert*-butyl iodide at 0 K is 17800 cm^{-1}.[49] Since there is not enough energy present at $\Delta v_{CH} = 6$ for direct dissociation, the observed process was indirect dissociation, likely involving a flow of energy from initially prepared CH vibrational overtone states into the vibrational bath via IVR. This redistributed energy eventually causes dissociation along the C−I bond. The process of dissociation was slow: it is estimated that the complete dissociation of the sample would take several hours at our current intracavity power levels if the scan range was restricted to 15200−16190 cm^{-1}. To minimize sample degradation, $\Delta v_{CH} = 6$ overtone spectra were gathered at a sampling rate such that each scan took 7 min and 30 s.

The typical energy range of a $\Delta v_{CH} = 7$ spectrum is 17600−19000 cm^{-1}, making the acquisition of vibrational overtone spectra impossible with our laboratory setup. Owing to the very high intracavity light levels, photodissociation occurred within seconds of introducing the PA sample cell into the laser cavity.

As in the case of *tert*-butyl chloride, the $\Delta v_{CH} = 2$ spectral region of *tert*-butyl iodide, seen in Figure 1, is too complex for local mode analysis. The $\Delta v_{CH} = 3$ spectral region in Figure 2 shows one transition to the pure local mode state $|0, 0\rangle|3\rangle$ (in the CH_d oscillator) at 8341 cm^{-1}. There is a local mode/local mode-normal mode combination pair involving the $|3, 0\rangle_{\pm}|0\rangle$ and $|2, 0\rangle_{\pm}|0\rangle + |nv_b\rangle$ states of the CH_u oscillator at 8496 and 8587 cm^{-1}, respectively. These three transitions comprise the most intense transitions observed at $\Delta v_{CH} = 3$. Fermi resonances similar to those observed in *tert*-butyl chloride (vide supra) were observed in all regions of the overtone spectrum of *tert*-butyl iodide. In Figure 3, we observe two Fermi resonances present between local modes and local mode-normal mode combination bands at $\Delta v_{CH} = 4$. The pure local mode transition $|0, 0\rangle|4\rangle$ occurs at 10852 cm^{-1} and is in resonance with the combination

TABLE 3: Pure Local Mode Transition Peak Properties of Vapor Phase *tert*-Butyl Iodide As Observed via ICL-PAS ($\Delta v_{CH} = 4-6$) and Conventional Absorption Spectroscopy ($\Delta v_{CH} = 3$)

Δv_{CH}	spectrometer/ laser	gas pressure (Torr)	bond	energy[a] (cm^{-1})	fwhm[a,b] (cm^{-1})
3	Cary 5e	15.4 ± 0.1	CH_u	8496, *8587*	43, *58*
			CH_d	8341	40
4	Ti:sapph (mw)	34.7 ± 0.8	CH_u	11113, *11181*	54, *59*
			CH_d	10852, *10890*	71, *38*
5	Ti:sapph (sw)	34.6 ± 0.7	CH_u	13 617	76
			CH_d	13 300	60
6	DCM dye	31.7 ± 0.3	CH_u	15 992	64
			CH_d	15551, *15618*	73, *72*

[a] Italicized values are for $|v - 1, 0, 0\rangle + |nv_b\rangle$. [b] Full width at half-maximum.

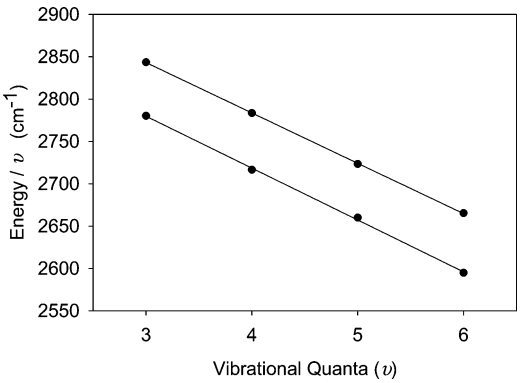

Figure 8. Birge−Sponer plots of the CH_u (top) and CH_d vibrational overtone transitions in *tert*-butyl iodide in the range $\Delta v_{CH} = 3-6$.

band $|0, 0\rangle|3\rangle + |nv_b\rangle$ at 10890 cm^{-1}. The pure local mode transition $|4, 0\rangle_{\pm}|0\rangle$ occurs at 11113 cm^{-1} and is in resonance with the combination band $|3, 0\rangle_{\pm}|0\rangle + |nv_b\rangle$ at 11181 cm^{-1}. These four transitions comprise the most intense transitions observed at $\Delta v_{CH} = 4$. The two sets of Fermi resonances that were observed at $\Delta v_{CH} = 4$ are seen to have coalesced at $\Delta v_{CH} = 5$ in Figure 4 (the low energy shoulder at 13216 cm^{-1} is different from the resonance observed at $\Delta v_{CH} = 4$). The pure local mode transition $|0, 0\rangle|5\rangle$ occurs at 13300 cm^{-1} while the other pure local mode transition $|5, 0\rangle_{\pm}|0\rangle$ occurs at 13617 cm^{-1}. The $\Delta v_{CH} = 6$ spectral region, seen in Figure 5, reveals the $|6, 0\rangle_{\pm}|0\rangle$ transition at 15992 cm^{-1}. The pure local mode transition $|0, 0\rangle|6\rangle$ occurs at 15551 cm^{-1} and is in resonance with a combination band $|0, 0\rangle|5\rangle + |nv_b\rangle$ (where the mode $|v_b\rangle$ is different from that observed at $\Delta v_{CH} = 5$) at 15618 cm^{-1}. A summary of the $\Delta v_{CH} = 3-6$ transitions of *tert*-butyl iodide can be seen in Table 3. Italicized values indicate the combination state $|v - 1, 0, 0\rangle + |nv_b\rangle$.

The data in Table 3 have been used to create Birge−Sponer plots, presented in Figure 8, for the CH_u and CH_d oscillators in *tert*-butyl iodide with peak centers (in the absence of Fermi resonance) approximated with eq 12. Local mode parameters $\tilde{\omega}$ and $\tilde{\omega}x$ were obtained via quadratic fits and Birge−Sponer regressions and are presented in Table 2. The $\tilde{\omega}$ values are higher for the more sterically crowded CH_u oscillator than for the less crowded CH_d oscillator. The anharmonicities of the "up" CH oscillators are smaller than those of the "down" oscillators, indicating that steric crowding may be rendering the CH_u stretching potential more harmonic than the CH_d stretching potential. In Table 2, we note that the $\tilde{\omega}$ value of the CH_d oscillator is significantly lower than those typically observed in other molecules. The $\tilde{\omega}$ value of the CH_u oscillator, which is comparable to that in *tert*-butyl chloride but otherwise atypically high, is attributed to a combination of steric crowding and a possible increase in the CH force constant by the halogen.[22,23]

There is a greater difference between the $\tilde{\omega}$ values of CH_u and CH_d in *tert*-butyl iodide than in *tert*-butyl chloride. This difference is correlated to the "separation" between the van der Waals spheres, δ, of H_u and the halide. The nuclear separations δ_{ClH} and δ_{IH}, calculated at HF/LanL2DZ, are used along with the van der Waals radii for hydrogen (120 pm), chlorine (180 pm), and iodine (215 pm) to obtain δ. These values are −6.5 and −13.5 pm for *tert*-butyl chloride and *tert*-butyl iodide, respectively. This greater steric crowding in *tert*-butyl iodide leads to a greater split between the $\tilde{\omega}$ values of CH_u and CH_d.

The photodissociation of *tert*-butyl iodide at $\Delta v_{CH} = 6$ did not proceed to any significant extent; i.e., dissociation products were not observed. The CH-containing daughter products of photodissociation would have had different local mode parameters, $\tilde{\omega}$ and $\tilde{\omega}x$, than the parent compound. Thus, if the photodissociation of *tert*-butyl iodide had proceeded to any significant extent we would expect to see a discontinuity in the Birge−Sponer plot between the $\Delta v_{CH} = 3-5$ sets of data points (where photodissociation was not observed) and the $\Delta v_{CH} = 6$ data points for the CH_d and/or CH_u oscillators. Since the Birge−Sponer data points at $\Delta v_{CH} = 6$ are not discontinuous with the $\Delta v_{CH} = 3-5$ sets of data points, and since the $\Delta v_{CH} = 6$ data points are derived from the most intense transitions at $\Delta v_{CH} = 6$, we conclude that photodissociation did not proceed to an appreciable degree during our spectral acquisition at this overtone.

Coupling Between Stretching and Torsional Motions. In the three molecules studied there is a 3-fold barrier to internal CH_3 rotation. Thus, the modulation of methyl $\tilde{\omega}$ and $\tilde{\omega}x$ with rotation about the internal methyl dihedral angle coordinate ϕ[50−54] is 3-fold. The dependence of $\tilde{\omega}$ and $\tilde{\omega}x$ on ϕ is approximated with a cosine squared function.[21] The equilibrium (staggered) conformers have a value of $\phi = 60°$ while the eclipsed conformers have a value of $\phi = 0°$.

Unscaled local mode frequencies of the staggered and eclipsed conformers, $\tilde{\omega}(60°)$ and $\tilde{\omega}(0°)$, and unscaled local mode anharmonicities, $\tilde{\omega}x(60°)$ and $\tilde{\omega}x(0°)$, were calculated from a fit of ab initio data in the range $r_e - 0.20$ Å to $r_e + 0.20$ Å in steps of 0.05 Å to eq 4. Calculations were carried out at HF/6-311+G(d,p) for the CH oscillators in *tert*-butyl chloride and at HF/LanL2DZ for the CH oscillators in *tert*-butyl chloride and *tert*-butyl iodide. Previously published data[55] were reanalyzed to obtain unscaled local mode frequencies and anharmonicities for neopentane and TMS at HF/6-311+G(d,p). As indicated above, the 6−311 basis set is not defined for iodine, therefore only the HF/LanL2DZ results are available for *tert*-butyl iodide.

The local mode frequencies and anharmonicities of the staggered conformers, $\tilde{\omega}(60°)$ and $\tilde{\omega}x(60°)$, were scaled[56] to the experimentally observed values of $\tilde{\omega}$ and $\tilde{\omega}x$. The $\tilde{\omega}(60°)$ scaling factor was applied to the unscaled value of $\tilde{\omega}(0°)$. Scaled values of $\tilde{\omega}(60°)$ and $\tilde{\omega}(0°)$ were used to calculate the values of the maximum variation of frequency with angle, $\delta_{\tilde{\omega}}$. Similarly, the $\tilde{\omega}x(60°)$ scaling factor was applied to the unscaled value of $\tilde{\omega}x(0°)$ to arrive at $\delta_{\tilde{\omega}x}$. The scaled values of $\tilde{\omega}$, $\tilde{\omega}x$, $\delta_{\tilde{\omega}}$, and $\delta_{\tilde{\omega}x}$ are given in Table 4. Scaling factors are specific to a given oscillator (e.g., CH, OH, etc.), molecule, ab initio method, q step-size, etc. and are given in Table 5. In addition to molecule-specific scaling factors for $\tilde{\omega}$ and $\tilde{\omega}x$, Table 5 also contains averaged local mode scaling factors for these CH oscillators and their standard deviations.

TABLE 4: Experimental[a] and Scaled ab Initio Calculated Local Mode Parameters for a Variety of Alkyl CH Oscillators Obtained from Quadratic Fits

		parameter (cm^{-1})					
molecule	bond	$\tilde{\omega}^a$	$\delta_{\tilde{\omega}}{}^b$	$\delta_{\tilde{\omega}}{}^c$	$\tilde{\omega}x^a$	$\delta_{\tilde{\omega}x}{}^b$	$\delta_{\tilde{\omega}x}{}^c$
tert-butyl chloride	CH_u	3085 ± 7	27.8	26.2	59.8 ± 1.2	−0.263	−0.0572
	CH_d	3047 ± 5	15.9	17.5	59.5 ± 0.9	0.274	0.288
tert-butyl iodide	CH_u	3080 ± 3		29.7	59.3 ± 0.5		0.145
	CH_d	3026 ± 9		29.1	61.5 ± 1.8		−0.126
neopentane-d_0		3049 ± 3^d	8.69		60.5 ± 0.4^d	0.232	
TMS		3042 ± 2^d	4.88		58.4 ± 0.3^d	0.0651	

[a] Obtained from a fit of experimental data to eq 3. [b] Calculated at HF/6-311+G(d,p). [c] Calculated at HF/LanL2DZ. [d] Raw data from ref 55 reanalyzed.

TABLE 5: Alkyl CH Oscillator Scaling Factors[a] Applied to the ab Initio Calculated Local Mode Parameters for the Molecules in Table 4

		local mode scaling factor			
molecule	bond	$sf(\tilde{\omega})^b$	$sf(\tilde{\omega})^c$	$sf(\tilde{\omega}x)^b$	$sf(\tilde{\omega}x)^c$
tert-butyl chloride	CH_u	0.952	0.935	0.85	0.80
	CH_d	0.950	0.935	0.85	0.80
tert-butyl iodide	CH_u		0.935		0.795
	CH_d		0.934		0.82
neopentane-d_0		0.9532		0.853	
TMS		0.9513		0.826	
av		0.9517	0.9351	0.845	0.804
std dev		0.0015	0.0005	0.013	0.010

[a] Suitable for relating ab initio calculated local mode parameters $\tilde{\omega}$, $\tilde{\omega}x$, $\delta_{\tilde{\omega}}$, and $\delta_{\tilde{\omega}x}$ to experimental values. [b] Calculated at HF/6-311+G(d,p). [c] Calculated at HF/LanL2DZ.

In Table 4 we note that the 6-311+G(d,p) and LanL2DZ basis sets agree well except for $\delta_{\tilde{\omega}x}$ of CH_u in *tert*-butyl chloride where LanL2DZ underestimates this value relative to 6-311+G(d,p). The most sterically hindered molecules were found to have, on average, the greatest $\delta_{\tilde{\omega}}$ values and the smallest $\delta_{\tilde{\omega}x}$ values. For neopentane and TMS, the net effect on the energy eigenvalues in eq 2 is a blue-shifting of the CH oscillators with increasing steric hindrance as the potential is rendered more harmonic by a barrier to high amplitude vibration. This blue-shifting is also apparent within the molecule *tert*-butyl chloride. Specifically, the more crowded oscillator, CH_u, has a higher $\delta_{\tilde{\omega}}$ value and smaller $\delta_{\tilde{\omega}x}$ value than does the less crowded CH_d oscillator. This is not the case, however, with *tert*-butyl iodide where the $\delta_{\tilde{\omega}}$ values are very similar for CH_u and CH_d, and the $\delta_{\tilde{\omega}x}$ of the former is higher than the latter. One possible reason for this anomalous behavior in *tert*-butyl iodide is that the LanL2DZ basis set *may* underestimate the $\delta_{\tilde{\omega}x}$ value of the CH_u oscillator (vide infra). As noted above, however, changes in the energy levels of the CH Morse oscillators are dominated by changes in $\tilde{\omega}$.

Predicting Local Mode Parameters Ab Initio. The relatively constant values of the individual scaling factors and the small standard deviations in the averaged values of $sf(\tilde{\omega})$ and $sf(\tilde{\omega}x)$ given in Table 5 indicate that it is possible to estimate the local mode parameters of alkyl CH oscillators with averaged scaling factors. An errors analysis indicates that uncertainties in the expansion terms f_{ii}, f_{iii}, and f_{iiii} (see eq 4) are the most significant contribution to the standard deviations of the averaged scaling factors, while uncertainties in the experimental values of $\tilde{\omega}$ and $\tilde{\omega}x$ (as reported in Table 2) are less important. The fitting process itself is therefore an important source of error, indicating that while expansions of the form of eq 4 are good approximations of the molecular potential energy surface as calculated ab initio, expansions in this functional form do introduce errors.

TABLE 6: Local Mode Scaling Factors[a] for ab Initio Calculated[b] Potential Energy Surfaces of a Test Set of Molecules

		polynomial[c]		nonlinear[d]	
molecule	bond	$sf(\tilde{\omega})$	$sf(\tilde{\omega}x)$	$sf(\tilde{\omega})$	$sf(\tilde{\omega}x)$
tert-butyl chloride	CH_u	0.9511	0.845	0.9440	0.927
	CH_d	0.9492	0.838	0.9421	0.920
neopentane[e]		0.9518	0.843	0.9449	0.925
TMS[e]		0.9497	0.816	0.9428	0.896
average		0.9499	0.839	0.9429	0.921
standard deviation		0.0016	0.014	0.0015	0.015

[a] Suitable for relating ab initio calculated local mode parameters $\tilde{\omega}$, $\tilde{\omega}x$, $\delta_{\tilde{\omega}}$, and $\delta_{\tilde{\omega}x}$ to experimental values. [b] Calculated at HF/6-311++G(2d,2p). [c] Obtained from fit of ab initio data to eq 4. [d] Obtained from fit of ab initio data to eq 1. [e] Raw data from ref 55 reanalyzed.

TABLE 7: Ab Initio[a] Local Mode Parameters for Alkyl CH Oscillators in *tert*-Butylbenzene[b]

	parameter (cm^{-1})			parameter (cm^{-1})	
bond	$\tilde{\omega}$	$\tilde{\omega}x$	bond	$\tilde{\omega}$	$\tilde{\omega}x$
$CH_{ip,u}$	3057 ± 5	60.2 ± 1.0	$CH_{op,d,f}$	3057 ± 5	60.0 ± 1.0
$CH_{ip,d}$	3059 ± 5	60.1 ± 1.0	$CH_{op,d,b}$	3073 ± 5	59.7 ± 1.0
$CH_{op,u}$	3046 ± 5	60.3 ± 1.0			

[a] Calculated at HF/6-311++G(2d,2p) and fit to eq 1 using the appropriate average scaling factors from Table 6. [b] C_s symmetry, carbon to methyl carbon bond in the plane of the benzene ring.

To investigate the role of the expansion form chosen to represent the ab initio CH stretching potential energy surface, individual and averaged scaling factors for ab initio calculated local mode parameters $\tilde{\omega}$ and $\tilde{\omega}x$ are calculated using both "polynomial" fit, i.e., the fit of energy to eq 4, and the "nonlinear" fit, i.e., fit of energy to eq 1. Calculations were carried out at HF/6-311++G(2d,2p) and the results are presented in Table 6. Both the polynomial and the nonlinear expansion forms are equally good approximations of the ab initio potential energy surface based upon the similar standard deviations of the local mode parameters. Extending the range of the ab initio data points from $q \in [-0.20, 0.20]$ Å to $q \in [-0.30, 0.30]$ Å (in steps of 0.05 Å) lead to no change in the standard deviations in the averaged local mode scaling factors.

The alkyl (methyl) local mode transition frequencies of *tert*-butylbenzene were predicted using eq 3 and the ab initio local mode parameters presented in Table 7. The subscript "ip" is used to denote CH bonds on the single in-plane methyl group while "op" denotes one of the two out-of-plane methyl groups which are gauche with respect to the benzene ring. Subscripts "u" and "d" refer to up- and down-orientation, where the former CH bonds are oriented at approximately 180° with respect to the benzene ring. The "d,f" (or "down, forward") CH bonds are those closer to the in-plane methyl while the "d,b" (or "down, backward") bonds are nearly parallel to the plane of the benzene ring.

TABLE 8: HCAO Calculated CH Vibrational Overtone Intensities in *tert*-Butyl Chloride and *tert*-Butyl Iodide

			tert-butyl chloride		*tert*-butyl iodide	
Δv_{CH}	bond	state	$\tilde{\nu}_{v\leftarrow 0}$[a]	f_{osc}[b]	$\tilde{\nu}_{v\leftarrow 0}$[a]	f_{osc}[b]
3	CH_u	$\|3, 0\rangle_{\pm}\|0\rangle$	8534	3.1 (3.7) × 10^{-8}	8528	2.1 (3.3) × 10^{-8}
	CH_d	$\|0, 0\rangle\|3\rangle$	8422	2.0 (2.2) × 10^{-8}	8340	1.4 (2.3) × 10^{-8}
4	CH_u	$\|4, 0\rangle_{\pm}\|0\rangle$	11142	2.8 × 10^{-9}	11134	3.9 × 10^{-9}
	CH_d	$\|0, 0\rangle\|4\rangle$	10993	1.9 × 10^{-9}	10874	2.8 × 10^{-9}
5	CH_u	$\|5, 0\rangle_{\pm}\|0\rangle$	13629	2.7 × 10^{-10}	13621	6.0 × 10^{-10}
	CH_d	$\|0, 0\rangle\|5\rangle$	13445	1.8 × 10^{-10}	13286	4.3 × 10^{-10}
6	CH_u	$\|6, 0\rangle_{\pm}\|0\rangle$	15998	3.1 × 10^{-11}	15989	9.7 × 10^{-11}
	CH_d	$\|0, 0\rangle\|6\rangle$	15778	2.1 × 10^{-11}	15574	6.8 × 10^{-11}
7	CH_u	$\|7, 0\rangle_{\pm}\|0\rangle$	18246	4.2 × 10^{-12}	18239	1.7 × 10^{-11}
	CH_d	$\|0, 0\rangle\|7\rangle$	17991	2.8 × 10^{-12}	17740	1.2 × 10^{-11}
8	CH_u	$\|8, 0\rangle_{\pm}\|0\rangle$	20375	6.9 × 10^{-13}	20370	3.4 × 10^{-12}
	CH_d	$\|0, 0\rangle\|8\rangle$	20086	4.5 × 10^{-13}	19782	2.4 × 10^{-12}
9	CH_u	$\|9, 0\rangle_{\pm}\|0\rangle$	22384	1.4 × 10^{-13}	22383	7.6 × 10^{-13}
	CH_d	$\|0, 0\rangle\|9\rangle$	22061	8.6 × 10^{-14}	21702.	5.4 × 10^{-13}

[a] Frequencies are in cm^{-1} and were calculated with the HCAO model. [b] Units are dimensionless oscillator strength. Values in parentheses are from experiment.

At $\Delta v_{CH} = 4$, the range of the predicted alkyl transition band centers is ca. 10980 ± 30 to 11100 ± 30 cm^{-1} while the observed range is ca. 10950−11070 cm^{-1}. This agreement is within experimental error, indicating that the ab initio local mode parameters in Table 7 may be appropriate for the alkyl oscillators in *tert*-butylbenzene. At $\Delta v_{CH} = 5$, the predicted alkyl transition range is ca. 13420 ± 40 to 13570 ± 40 cm^{-1} while the observed range is ca. 13500 to 13650 cm^{-1}. There appears to be a small red-shifting of the predicted alkyl transitions at $\Delta v_{CH} = 5$. It is reasonable that, in scaling ab initio local mode parameters, different scaling factors should be used for modes which are more sterically crowded than others.

HCAO Intensities. To ensure a reasonable mapping of the potential energy surface, DMFs should be calculated using at least nine grid points with a step size of 0.05 Å.[57] The HCAO intensities presented in this paper were calculated using 11 grid points in the range $q \in [-0.30, 0.30]$ Å, with a step size of 0.05 Å. The HF wave functions are stable provided that $|q| \leq 0.50$ Å.[48]

The calculation of HCAO intensities in *tert*-butyl chloride and *tert*-butyl iodide require the values of the intramanifold coupling constants for (symmetric) $CH_u\cdots CH_u$ coupling and for (asymmetric) $CH_u\cdots CH_d$ coupling, denoted γ'_{12} and γ'_{13}, respectively. These values could not be obtained from ab initio vibrational frequency calculations as the anticipated rms errors in calculated vibrational frequency are greater than the coupling constants themselves.

Ahmed and Henry[24] have reported a γ'_{12} value of 12.0 cm^{-1} for *tert*-butyl chloride. To evaluate γ'_{13}, we begin with the value of γ_{12} obtained from the ab initio calculated H_u-C-H_u bond angle θ_{12} and eq 11. Next, γ_{12} is used with the published value $\gamma'_{12} = 12.0$ cm^{-1} in eq 8 to obtain ϕ_{12}. We assume that the symmetric and asymmetric potential energy coupling terms given by eq 9, ϕ_{12} and ϕ_{13}, are identical. Finally, the intramanifold coupling γ'_{13} is obtained from eq 8 using ϕ_{13} and γ_{13} from eq 11 (where θ_{13} is the ab initio calculated H_u-C-H_d bond angle). The local mode parameters in Table 2 and bond angles calculated at HF/6-311++G(2d,2p) lead to $\gamma'_{13} = 13.4$ cm^{-1} for *tert*-butyl chloride. Note that in eq 8 the local mode frequencies for *tert*-butyl chloride are $\tilde{\omega}_1 = \tilde{\omega}_2 = 3085$ cm^{-1} and $\tilde{\omega}_3 = 3044$ cm^{-1}.

The infrared spectrum of *tert*-butyl iodide[58] shows the CH stretching transitions occur at 2909.2 cm^{-1} ($|1\rangle_s$), 2967 cm^{-1} ($|10\rangle_{+a}$), and 2974.3 cm^{-1} ($|10\rangle_{-a}$). Taking the coupling constant γ'_{12} to be twice the splitting between the $|10\rangle_{-a}$ and $|10\rangle_{+a}$ states we arrive at $\gamma'_{12} = 3.6$ cm^{-1}. Using an approach identical to that used to obtain γ'_{13} for *tert*-butyl chloride (vide supra), we find that $\gamma'_{13} = 6.2$ cm^{-1} for *tert*-butyl iodide.

The experimental and HCAO calculated intensities for vibrational overtone transitions in *tert*-butyl chloride and *tert*-butyl iodide are given in Table 8. The HCAO intensities were calculated from eq 15 using Morse wave functions[11] obtained from the Birge−Sponer experimental local mode parameters for the CH_u and CH_d oscillators from Table 2 and fourth order polynomial approximations (eq 16) to the DMFs. These DMFs were calculated from ab initio data points at HF/6-311++G-(2d,2p) for *tert*-butyl chloride and at HF/LanL2DZ for *tert*-butyl iodide. HCAO calculated intensity for *tert*-butyl chloride underestimates the experimental intensities for $|3, 0\rangle_{\pm}|0\rangle$ and $|0, 0\rangle|3\rangle$ by 16% and 10%, respectively, at the HF/6-311++G-(2d,2p) level. The HCAO calculated intensities were also calculated at HF/LanL2DZ and were found to be significantly worse. The HF/LanL2DZ HCAO intensities are not presented. HCAO calculated intensities for *tert*-butyl iodide underestimate the experimental intensities at the HF/LanL2DZ level.

Conclusion

Ab initio calculated geometries and van der Waals radii have been used as crude metrics to quantify the relative degree of steric crowding in the molecules *tert*-butylbenzene, *tert*-butyl chloride, and *tert*-butyl iodide. All of these molecules have sterically hindered CH oscillators in the sense that they possess hydrogen atoms which are separated from proximal atoms (e.g., H, Cl, or I) to which they are not chemically bound by less than the sum of their van der Waals radii. The stretching vibrational overtone spectra of these crowded CH oscillators showed evidence of through-space interactions between CH oscillators and proximal atoms (e.g., H, Cl, and I) to which the oscillator was not bound. Specifically, CH stretching frequencies were found to increase with increased steric crowding (vide infra).

The vibrational overtone spectrum of *tert*-butylbenzene in the energy regime $\Delta v_{CH} = 2-7$ was found to be very complex. The presence of 10 unique CH oscillators in *tert*-butylbenzene made the overtone spectra impossible to assign.

The vibrational overtone spectrum of *tert*-butyl chloride was obtained in the $\Delta v_{CH} = 2-7$ regions. The spectra exhibited simple, well-behaved Fermi resonances. *tert*-Butyl chloride contains three "down" CH_d oscillators and six "up" CH_u oscillators which were resolved in the vibrational overtone spectrum. The local mode parameters of CH_u were determined

to be $\tilde{\omega} = 3084 \pm 4$ cm^{-1} and $\tilde{\omega}x = 59.6 \pm 0.8$ cm^{-1} while those of of CH_d were determined to be $\tilde{\omega} = 3044 \pm 3$ cm^{-1} and $\tilde{\omega}x = 59.0 \pm 0.6$ cm^{-1}. The interoscillator coupling term between CH_u oscillators was $\gamma'_{12} = 12.0$ cm^{-1} while that between CH_u and CH_d oscillators was calculated to be $\gamma'_{13} = 13.4$ cm^{-1}. These parameters were used along with the HCAO model and a DMF calculated at HF/6-311++G(d,p) to obtain calculated vibrational overtone transition intensities in the range $\Delta v_{CH} = 3-9$.

tert-Butyl iodide decomposed instantaneously at $\Delta v_{CH} = 7$. The vibrational overtone spectrum was obtained in the $\Delta v_{CH} = 2-6$ regions. The spectra exhibited simple, well-behaved Fermi resonances. The CH_d and CH_u oscillators were resolved in the vibrational overtone spectrum. The local mode parameters of CH_u were determined to be $\tilde{\omega} = 3081 \pm 2$ cm^{-1} and $\tilde{\omega}x = 59.5 \pm 0.3$ cm^{-1} while those of of CH_d were determined to be $\tilde{\omega} = 3025 \pm 5$ cm^{-1} and $\tilde{\omega}x = 61.3 \pm 1.1$ cm^{-1}. The interoscillator coupling term γ'_{12} was 3.6 cm^{-1} while γ'_{13} was 6.2 cm^{-1}. These parameters were used along with the HCAO model and a DMF calculated at HF/LanL2DZ to obtain calculated vibrational overtone transition intensities in the range $\Delta v_{CH} = 3-9$.

The experimental local mode parameters for *tert*-butyl chloride and *tert*-butyl iodide, along with those previously obtained for neopentane and TMS, were used to obtain scaling factors to relate ab initio calculated local mode parameters to their experimental values. The small standard deviations between molecule specific scaling factors made it possible to obtain averaged scaling factors for a general, nonmolecule specific alkyl CH oscillator. These general scaling factors are specific to a given level of theory, basis set, step size, and the functional form used to approximate the CH stretching potential. Both a Taylor series expansion and a Morse function were found to be equally good approximations of the ab initio calculated CH stretching potential.

Local mode-torsion coupling terms were calculated for *tert*-butyl chloride, *tert*-butyl iodide, neopentane, and TMS. There was a general blue-shifting of hindered oscillators which correlated approximately with the height of the barrier to internal methyl rotation. The blue-shifting was manifested as an increase in the local mode frequency-torsion coupling term, $\delta_{\tilde{\omega}}$, and in some cases as a decrease in the local mode anharmonicity-torsion coupling term, $\delta_{\tilde{\omega}x}$. That is, CH stretching frequencies were found to increase with increased steric crowding, and in some instances, local mode anharmonicities were found to decrease with increasing crowding. In general, the more sterically hindered a CH oscillator, the more harmonic its stretching potential is rendered.

Acknowledgment. The authors wish to acknowledge the use of SHARCNET's computational resources and the assistance of SHARCNET's technical support staff. Funding for this research has been provided by the Natural Sciences and Engineering Council of Canada.

References and Notes

(1) Mecke, R.; Ziegler, R. *Z. Phys.* **1936**, *101*, 405.
(2) Hayward, R. J.; Henry, B. R. *J. Mol. Spectrosc.* **1975**, *57*, 221.
(3) Henry, B. R. *Acc. Chem. Res.* **1977**, *10*, 207.
(4) Watson, I. A.; Henry, B. R.; Ross, I. G. *Spectrochim. Acta A* **1981**, *37A*, 857.
(5) Mortensen, O. S.; Henry, B. R.; Mohammadi, M. A. *J. Chem. Phys.* **1981**, *75*, 4800.
(6) Henry, B. R.; Gough, K. M.; Sowa, M. G. *Int. Rev. Phys. Chem.* **1986**, *5*, 133.
(7) Henry, B. R.; Swanton, D. J. *J. Mol. Struct.* **1989**, *202*, 193.
(8) Kjaergaard, H. G.; Proos, R. J.; Turnbull, D. M.; Henry, B. R. *J. Phys. Chem.* **1996**, *100*, 19273.
(9) Swofford, R. L.; Long, M. E.; Albrecht, A. C. *J. Chem. Phys.* **1976**, *65*, 179.
(10) Henry, B. R. *Acc. Chem. Res.* **1987**, *20*, 429.
(11) Sage, M. L.; Jortner, J. *Adv. Chem. Phys.* **1981**, *47*, 293.
(12) Nesbitt, D. J.; Field, R. W. *J. Phys. Chem.* **1996**, *100*, 12735.
(13) Elert, M. L.; Stannard, P. R.; Gelbart, W. M. *J. Chem. Phys.* **1977**, *67*, 5395.
(14) Sage, M. L. *Chem. Phys.* **1978**, *35*, 375.
(15) Child, M. S.; Lawton, T. R. *Faraday Discuss. Chem. Soc.* **1981**, *71*, 273.
(16) Henry, B. R.; Tarr, A. W.; Mortensen, O. S.; Murphy, W. F.; Compton, D. A. C. *J. Chem. Phys.* **1983**, *79*, 2583.
(17) Child, M. S.; Halonen, L. *Adv. Chem. Phys.* **1984**, *57*, 1.
(18) Henry, B. R.; Miller, R. J. D. *Chem. Phys. Lett.* **1978**, *60*, 81.
(19) Mohammadi, M. A.; Henry, B. R. *Proc. Natl. Acad. Sci. U.S.A.* **1981**, *78*, 686.
(20) Henry, B. R.; Mohammadi, M. A.; Thomson, J. A. *J. Chem. Phys.* **1981**, *75*, 3165.
(21) Petryk, M. W. P.; Henry, B. R. *J. Phys. Chem. A* **2002**, *106*, 8599.
(22) Kaye, W. *Spectrochim. Acta* **1954**, *6*, 257.
(23) Henry, B. R.; Hung, I.-F. *Chem. Phys.* **1978**, *29*, 465.
(24) Ahmed, M. K.; Henry, B. R. *J. Phys. Chem.* **1987**, *91*, 3741.
(25) Henry, B. R.; Sowa, M. G. *Prog. Anal. Spectrosc.* **1989**, *12*, 349.
(26) Henry, B. R.; Kjaergaard, H. G.; Neifer, B.; Schattka, B. J.; Turnbull, D. M. *Can. J. Appl. Spectrosc.* **1993**, *38*, 42.
(27) Rothman, L. S.; Gamache, R. R.; Tipping, R. H.; Rinsland, C. P.; Smith, M. A. H.; Benner, D. C.; Devi, V. M.; Flaund, J.-M.; Camy-Peyret, C.; Perrin, A.; Goldman, A.; Massie, S. T.; Brown, L. R.; Toth, R. A. *J. Quant. Spectrosc. Radiat. Transfer* **1992**, *48*, 469.
(28) Henry, B. R. The Local Mode Model. In *Vibrational Spectra and Structure*; Durig, J. R., Ed.; Elsevier Scientific: Amsterdam, 1981; Vol. 10.
(29) Sowa, M. G.; Henry, B. R.; Mizugai, Y. *J. Phys. Chem.* **1991**, *95*, 7659.
(30) Boyarkin, O. V.; Rizzo, T. R.; Perry, D. S. *J. Chem. Phys.* **1999**, *110*, 11346.
(31) Fermi, E. *Z. Phys.* **1931**, *71*, 250.
(32) Perry, J. W.; Moll, D. J.; Kuppermann, A.; Zewail, A. H. *J. Chem. Phys.* **1985**, *82*, 1195.
(33) Atkins, P. W. *Molecular Quantum Mechanics*, 2nd ed.; Oxford University Press: Oxford, U.K., 1983.
(34) Cohen, E. R.; Taylor, B. N. *J. Res. Natl. Bur. Stand.* **1987**, *92*, 85.
(35) Kjaergaard, H. G. Local Mode Spectroscopy: Calculation and Measurement of Overtone Intensities. Thesis, Odense Univerity, 1992.
(36) Kjaergaard, H. G.; Yu, H.; Schattka, B. J.; Henry, B. R.; Tarr, A. W. *J. Chem. Phys.* **1990**, *93*, 6239.
(37) Mortensen, O. S.; Ahmed, M. K.; Henry, B. R.; Tarr, A. W. *J. Chem. Phys.* **1985**, *82*, 3903.
(38) Tarr, A. W.; Swanton, D. J.; Henry, B. R. *J. Chem. Phys.* **1986**, *85*, 3463.
(39) Kjaergaard, H. G.; Henry, B. R.; Tarr, A. W. *J. Chem. Phys.* **1991**, *94*, 5844.
(40) Frisch, M. J.; Trucks, G. W.; Schlegel, H. B.; Scuseria, G. E.; Robb, M. A.; Cheeseman, J. R.; Zakrzewski, V. G.; Montgomery, J. A., Jr.; Stratmann, R. E.; Burant, J. C.; Dapprich, S.; Millam, J. M.; Daniels, A. D.; Kudin, K. N.; Strain, M. C.; Farkas, O.; Tomasi, J.; Barone, V.; Cossi, M.; Cammi, R.; Mennucci, B.; Pomelli, C.; Adamo, C.; Clifford, S.; Ochterski, J.; Petersson, G. A.; Ayala, P. Y.; Cui, Q.; Morokuma, K.; Malick, D. K.; Rabuck, A. D.; Raghavachari, K.; Foresman, J. B.; Cioslowski, J.; Ortiz, J. V.; Stefanov, B. B.; Liu, G.; Liashenko, A.; Piskorz, P.; Komaromi, I.; Gomperts, R.; Martin, R. L.; Fox, D. J.; Keith, T.; Al-Laham, M. A.; Peng, C. Y.; Nanayakkara, A.; Gonzalez, C.; Challacombe, M.; Gill, P. M. W.; Johnson, B.; Chen, W.; Wong, M. W.; Andres, J. L.; Gonzalez, C.; Head-Gordon, M.; Replogle, E. S.; Pople, J. A. Gaussian 98, Revision A.5. 1998.
(41) Frisch, M. J.; Trucks, G. W.; Schlegel, H. B.; Scuseria, G. E.; Robb, M. A.; Cheeseman, J. R.; Zakrzewski, V. G.; Montgomery, J. A., Jr.; Stratmann, R. E.; Burant, J. C.; Dapprich, S.; Millam, J. M.; Daniels, A. D.; Kudin, K. N.; Strain, M. C.; Farkas, O.; Tomasi, J.; Barone, V.; Cossi, M.; Cammi, R.; Mennucci, B.; Pomelli, C.; Adamo, C.; Clifford, S.; Ochterski, J.; Petersson, G. A.; Ayala, P. Y.; Cui, Q.; Morokuma, K.; Salvador, P.; Dannenberg, J. J.; Malick, D. K.; Rabuck, A. D.; Raghavachari, K.; Foresman, J. B.; Cioslowski, J.; Ortiz, J. V.; Baboul, A. G.; Stefanov, B. B.; Liu, G.; Liashenko, A.; Piskorz, P.; Komaromi, I.; Gomperts, R.; Martin, R. L.; Fox, D. J.; Keith, T.; Al-Laham, M. A.; Peng, C. Y.; Nanayakkara, A.; Challacombe, M.; Gill, P. M. W.; Johnson, B.; Chen, W.; Wong, M. W.; Andres, J. L.; Gonzalez, C.; Head-Gordon, M.; Replogle, E. S.; Pople, J. A. Gaussian 98, Revision A.11. 2001.
(42) Frisch, M. J.; Trucks, G. W.; Schlegel, H. B.; Scuseria, G. E.; Robb, M. A.; Cheeseman, J. R.; Montgomery, J. A., Jr.; Vreven, T.; Kudin, K. N.; Burant, J. C.; Millam, J. M.; Iyengar, S. S.; Tomasi, J.; Barone, V.;

Mennucci, B.; Cossi, M.; Scalmani, G.; Rega, N.; Petersson, G. A.; Nakatsuji, H.; Hada, M.; Ehara, M.; Toyota, K.; Fukuda, R.; Hasegawa, J.; Ishida, M.; Nakajima, T.; Honda, Y.; Kitao, O.; Nakai, H.; Klene, M.; Li, X.; Knox, J. E.; Hratchian, H. P.; Cross, J. B.; Adamo, C.; Jaramillo, J.; Gomperts, R.; Stratmann, R. E.; Yazyev, O.; Austin, A. J.; Cammi, R.; Pomelli, C.; Ochterski, J. W.; Ayala, P. Y.; Morokuma, K.; Voth, G. A.; Salvador, P.; Dannenberg, J. J.; Zakrzewski, V. G.; Dapprich, S.; Daniels, A. D.; Strain, M. C.; Farkas, O.; Malick, D. K.; Rabuck, A. D.; Raghavachari, K.; Foresman, J. B.; Ortiz, J. V.; Cui, Q.; Baboul, A. G.; Clifford, S.; Cioslowski, J.; Stefanov, B. B.; Liu, G.; Liashenko, A.; Piskorz, P.; Komaromi, I.; Martin, R. L.; Fox, D. J.; Keith, T.; Al-Laham, M. A.; Peng, C. Y.; Nanayakkara, A.; Challacombe, M.; Gill, P. M. W.; Johnson, B.; Chen, W.; Wong, M. W.; Gonzalez, C.; Pople, J. A. Gaussian 03, Revision B.03. 2003.

(43) SpectraCalc is commercially available software from Galactic Industries Corporation.

(44) Pauling, L. *The Nature of the Chemical Bond*, 3rd ed.; Cornell University Press: Ithaca, NY, 1960.

(45) Henry, B. R.; Siebrand, W. *J. Chem. Phys.* **1968**, *49*, 5369.

(46) Fang, H. L.; Swofford, R. L. *J. Chem. Phys.* **1980**, *72*, 6382.

(47) Henry, B. R.; Mohammadi, M. A. *Chem. Phys.* **1981**, *55*, 385.

(48) Petryk, M. W. P. Local Mode Vibrational Overtones Of Sterically Crowded Molecules. Thesis, University of Guelph, 2004.

(49) Kim, Y. S.; Kang, W. K.; Kim, D.-C.; Jung, K.-H. *J. Phys. Chem. A* **1997**, *101*, 7576.

(50) Zhu, C.; Kjaergaard, H. G.; Henry, B. R. *J. Chem. Phys.* **1997**, *107*, 691.

(51) Kjaergaard, H. G.; Turnbull, D. M.; Henry, B. R. *J. Phys. Chem. A* **1998**, *102*, 6095.

(52) Cavagnat, D.; Lespade, L. *J. Chem. Phys.* **1997**, *106*, 7946.

(53) Cavagnat, D.; Lespade, L. *J. Chem. Phys.* **1998**, *108*, 9275.

(54) Lapouge, C.; Cavagnat, D. *J. Phys. Chem. A* **1998**, *102*, 8393.

(55) Petryk, M. W. P.; Henry, B. R. *Can. J. Chem.* **2001**, *79*, 279.

(56) Low, G. R.; Kjaergaard, H. G. *J. Chem. Phys.* **1999**, *110*, 9104.

(57) Low, G. R. Calculation of OH−Stretching Vibrational Properties of Water Clusters. Thesis, University of Otago, 2001.

(58) McKean, D. C.; Biedermann, S.; Bürger, H. *Spectrochim. Acta A* **1974**, *30A*, 845.